International Journal of Low-Carbon Technologies Advance Access published December 28, 2013

Quantification and mitigation of long-term impacts of urbanization and climate change in the tropical coastal city of San Juan, Puerto Rico

Daniel E. Comarazamy[1], Jorge E. González[2*] and Jeffrey C. Luvall[3]

[1]The NOAA-CREST Center, The City College of New York, New York, NY, USA
[2]The NOAA-CREST Center and Department of Mechanical Engineering, The City College of New York, New York, NY, USA; [3]Global Hydrology and Climate Center, NASA Marshall Space Flight Center, Huntsville, AL, USA

Abstract

Urbanization, along with other cases of land cover and land use changes, has significant climate impacts in tropical regions with the added complexity of occurring within the context of global warming (GW). The individual and combined effects of these two factors on the surface energy balance of a tropical city are investigated by the use of an integrated atmospheric modeling approach, taking the San Juan Metropolitan Area (SJMA), Puerto Rico, as the test case. To achieve this goal, an ensemble of climate and weather simulations is performed, with climate scenarios combining urban development and sprawl with regional climate change over the past 50 years and the short-term simulations designed to test the sensitivity to different urban vegetation configurations as mitigating alternatives. As indicator of change, we use the thermal response number (TRN), which is a measure of the sensible heating to the thermal storage of a surface or region, and the Bowen ratio, which is defined as the ratio of sensible to latent heat fluxes. The TRN of the area occupied by the SJMA has decreased as a consequence of replacing the lowland coastal plain vegetation with man-made materials, indicating that it takes less energy to raise the surface temperature of the urban area, whereas the TRN of forested regions has remained virtually unchanged. The GW signal also has effects on the thermal response of the SJMA, where dryer current conditions generate lower TRN values. Differences owing to GW are more evident in the Bowen ratio pattern, mostly associated with the drier present conditions observed and its effects on sensible and latent heat fluxes. In terms of testing different mitigation strategies, the short-term simulations show that the urban area is more efficient in partitioning surface energy balance terms when green roofs are specified, as opposed to including vegetation inside the urban core.

Keywords: urbanization; remote sensing; mitigation; global warming.

*Corresponding author:
gonzalez@me.ccny.cuny.edu

Received 23 January 2013; revised 30 April 2013; accepted 7 July 2013

1 INTRODUCTION

Urbanization is one of the most extreme cases of environmental and land cover and land use (LCLU) change. It has been the focal point of both policymaking and scientific research over recent years. The impacts of urbanization, ranging from global, to regional, to local scales, include, but are not limited to, changes in atmospheric composition and radiative forcing, global warming (GW), effects on the water cycle and surface energy balance, and ecosystems modifications. A clearest indicator of climate changes owing to urbanization is a well-known urban/rural convective circulation known as urban heat islands (UHIs). The UHI is defined as a dome of high temperatures observed over urban centers as compared with the relatively low temperatures of the rural surroundings [1, 2].

Some factors that lead to the formation of a heat island include the widespread use of diverse construction materials, such as concrete, asphalt, steel and glass, among many others.

International Journal of Low-Carbon Technologies 2013, 0, 1–11

doi:10.1093/ijlct/ctt059

Materials used in cities have a much higher thermal inertia than natural vegetation-covered surfaces, resulting in large differences in temperature during the first several hours after sundown, when all the energy absorbed and stored during daylight is released to the lower atmosphere over the city. Tall, vertical surfaces and other geometric shapes of the urban landscape create what is known as the canyon effect [3–5]. In the spaces between buildings, longwave radiation emitted by the surface at night is reflected and absorbed by the walls, resulting in trapped energy and higher temperatures. The urban landscape also interrupts wind flows and results in decreased heat loss. Paved surfaces prevent precipitation from entering the soil and subsoil, resulting in less moisture available in green areas for evapotranspiration, a non-radiative air-cooling phenomenon. These temperature contrasts are greater in clear and calm conditions and tend to disappear in cloudy and windy weather by the effects of thermal and mechanical mixing.

The UHI was first recognized in London in 1820 when observations showed that the city was up to 2.1°C warmer at night than the surrounding countryside and up to 0.19°C cooler during the day [1]. Since then it has been widely studied and UHIs of diverse magnitude, its causes and patterns, have been reported for a number of cities along with some of its most important regional and local effects (e.g. [1, 6–13]; among many others). The majority of these previous studies rely on observational station data and satellite information, simplified numerical simulations and idealized laboratory experiments and focus on large continental cities, generally located in northern temperate regions, and although the general UHI pattern reported is similar, each city is exposed to diverse local and synoptic factors, which causes the study of UHI to be complex and specific of the locality. UHIs in tropical regions have been identified in Kuala Lumpur, Malaysia, the island state of Singapore [14], and in San Juan, Puerto Rico [15], by comparing historical temperature differences between urban centers and their rural surroundings, followed by numerical simulations.

Studies of LCLU change, which includes urbanization and deforestation, and its associated climatic impacts in tropical coastal regions, have been limited. It was recently reported that lowland deforestation is leading to increases in cloud base heights and thinner clouds in rain forests in Central America [16–18], which is resulting in increases in regional droughts. However, a similar study using numerical analysis conducted in Puerto Rico reported an increase in cloud base height, but using a forested island [19, 20]. The discrepancy on the results by these two studies is addressed in Ray et al. [18] and settled by explaining that the effect on cloud base height is linked to the net effect the LCLU change has on the local Bowen ratio, the ratio of energy fluxes from the ground to the atmosphere by sensible and latent heating, respectively. A recent study found that the combined effect of LCLU changes and GW was to produce higher cloud bases, less atmospheric water content in the vertical column and widespread precipitation decreases in northeastern Puerto Rico [21]. Velazquez-Lozada et al. [15] conducted an observational and numerical study that proved the existence of an UHI for the tropical coastal city of San Juan, Puerto Rico, and some of its local patterns. They found that larger temperature differences between the city and the surrounding countryside were more noticeable during the Caribbean Dry and early rainfall seasons (ERSs), which together comprise the period from December to June [22, 23] (Figure 1).

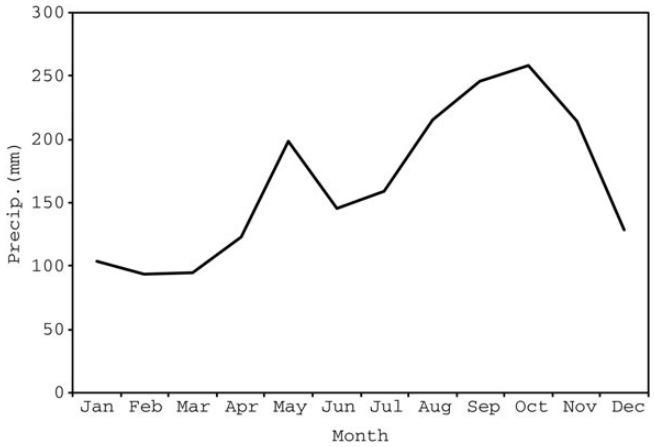

Figure 1. *30-year (1970–2000) monthly precipitation climatology for 15 COOP stations distributed throughout Puerto Rico (adapted from [42]).*

These results motivated the development of more extensive and wide-ranging experimental campaigns and integrated numerical experiments with the objective of determining the particular characteristics of the San Juan Metropolitan Area (SJMA) UHI and investigating the possible impacts of LCLU changes in tropical coastal regions. The first of these field campaigns was designated as the San Juan Atlas Mission, which took place on 11–16 February 2004 and combined remote sensing, surface observations, upper air analyses and mesoscale numerical modeling [24, 25]. Data from weather stations and temperature sensors deployed during the Atlas Mission revealed a strong daytime UHI consistently ranging between 7 and 9°C and heavily influenced by the occurrence of short-lived and weak precipitation events, apparently modulated by the availability of soil moisture within the urban area and the thermal inertia of wet soil (both in the city and the surrounding rural areas). These conclusions are in agreement with observational studies of UHI characteristics performed at different climate zones [26], where it was found that daytime UHIs in wet climates are larger than nighttime values owing to the high thermal inertia of wet rural soils. The high-resolution remote-sensing information obtained during the Atlas Mission was used to identify the geographical extension of the SJMA and to update the surface characteristics available in regional models to obtain a detailed, heterogeneous configuration of the SJMA [27]. The Regional Atmospheric Modeling System (RAMS), driven with global reanalysis data for a 10-day simulation, yielded satisfactory results in near-surface air temperatures and vertical profiles of temperatures and wind speeds.

Whereas these past studies focused on the climate impact due to one factor with the consensus in each study that they had limited scope and analysis and were too simplified in their atmospheric modeling approach and more work needed to be done, here we present the climate impacts due to LCLU change and GW on the partitioning of surface energy balance terms, while also

exploring the effectiveness of different proposed mitigation techniques to the effects of UHI, taking the tropical coastal city of San Juan, Puerto Rico, as the test case. In the next section, the methodology used in this research is presented, which employs a regional atmospheric model as the main research tool. The atmospheric model chosen is RAMS; results from control runs were validated for accuracy and reliability against observations [21, 27, 28]. Section 2 also includes a description of the LCLU and climate data used, and the main simulation matrix executed. In Section 3, the thermal response number (TRN) is introduced, followed by the study of the individual and combined effects of LCLU changes and GW on the surface energy balance of San Juan, Puerto Rico, and an investigation on the effectiveness of green roofs, tree-lined streets and city-wide parks as mitigating alternatives (Section 4). Finally, a summary of the major findings of this research is presented, with recommendations for future work, possible implications in related fields.

2 METHODOLOGY

Given the importance of tropical coastal cities and the relatively lack of studies that include all contributing factors leading to local climate changes at resolutions fine enough to draw strong conclusions, the research presented in this paper is an attempt at quantifying the possible impacts of LCLU changes on surface energy partitioning in a tropical coastal city under conditions of GW and to quantify possible mitigating strategies to reduce these impacts.

2.1 Experimental set-up and datasets

To achieve the above-stated goals, numerical simulations are configured combining two LCLU scenarios (representing current and pre-urban conditions) with two large-scale atmospheric conditions (representing different periods of GW and their corresponding levels of greenhouse gases emissions), resulting in the run matrix in Table 1. The timeframe for the present and past climatologies were selected to reduce the influence of El Niño–Southern Oscillation (ENSO) and North Atlantic Oscillation (NAO) on the Caribbean ERS climate, as identified by previous studies (e.g. [23, 29, 30]), and in accordance with periods of urban development that still presented a significant climate change in the region of interest. The five-year periods from 1955 to 1959 (Pre-GW) and 2000 to 2004 (GW) are the best available in the long-term record, in terms of ENSO and NAO indices, to perform the simulations [21]. Both atmospheric conditions were dynamically downscaled from the NCEP 2.5° Reanalysis data [31], with SST specifications derived from Smith and Reynolds Extended Reconstruction Sea Surface Temperatures (ERSSTs v3b) [32, 33].

Digital maps of LCLU available for 1951 and 2000 [34] were analyzed to verify that urban development and LCLU changes are in accordance with the two timeframes selected and then were configured for the simulations. The first step in this configuration consists of a reclassification of LCLU classes to match the modeling grids (Figure 2) and the land classification index system in the atmospheric model [35] (Table 2). This way, the LCLU specifications used as surface characteristics for the simulations driven with past and present atmospheric and oceanic conditions were obtained (Figure 3). The methods to derive the 1951 and 2000 LCLU specifications differ only in the use of high-resolution remote-sensing data for the SJMA, Caguas, El Yunque and surrounding areas obtained with the Airborne Thermal and Land Applications Sensor (ATLAS) instrument [25] to complement the present LCLU dataset. More details on

Table 1. *Simulation matrix.*

Run ID	LCLU	Driving conditions
PRESENT1[a]	2000 + ATLAS	2000–04 atmospheric and oceanic conditions
PRESENT2	2000 + ATLAS	1955–59 atmospheric and oceanic conditions
PAST1	1951 (Pre-urban)	2000–04 atmospheric and oceanic conditions
PAST2[a]	1951 (Pre-urban)	1955–59 atmospheric and oceanic conditions
ATLAS–GREEN	2000 + ATLAS	February 10–12, 2012, twice-daily upper air radiosonde
ATLAS-TREES	2000 + ATLAS	February 10–12, 2012 twice-daily upper air radiosonde
ATLAS-PARKS	2000 + ATLAS	February 10–12, 2012 twice-daily upper air radiosonde
ATLAS	2000 + ATLAS	February 10–12, 2012 twice-daily upper air radiosonde

[a]Serve as control runs to test model accuracy.

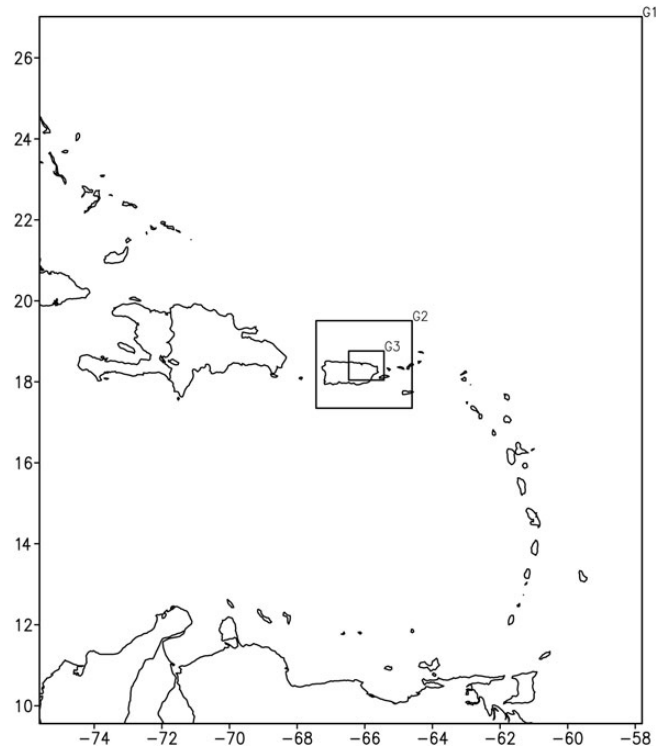

Figure 2. *Locations of modeling grids used in this research. Grid 1 (G1), showing the Caribbean Basin and islands, Grid 2 (G2) covers the island of Puerto Rico and adjoining islands and Grid 3 (G3) covers the northeastern region of Puerto Rico, the main area of interest in this research.*

Table 2. *LEAF-2 biophysical parameters by land use class number.*

No.	Description	Albedo	emissivity	Lai	vfrac	zo	zdisp	rootdep
0	Ocean	0.14	0.99	0.0	0.00	0.00	0.1	0.0
1	Inland water	0.14	0.99	0.0	0.00	0.00	0.1	0.0
2	Ice/glacier	0.40	0.82	0.0	0.00	0.01	0.1	0.0
3	Evergreen needleleaf tree	0.10	0.97	6.0	0.80	1.00	15.0	1.5
4	Deciduous needleleaf tree	0.10	0.95	6.0	0.80	1.00	20.0	1.5
5	Deciduous broadleaf tree	0.20	0.95	6.0	0.80	0.80	15.0	2.0
6	Evergreen broadleaf tree	0.15	0.95	6.0	0.90	2.00	20.0	1.5
7	Short grass	0.26	0.96	2.0	0.80	0.02	0.2	1.0
8	Tall grass	0.16	0.96	6.0	0.80	0.10	1.0	1.0
9	Desert	0.30	0.86	0.0	0.00	0.05	0.1	1.0
10	Semi-desert	0.25	0.96	6.0	0.10	0.10	0.5	1.0
11	Tundra	0.20	0.95	6.0	0.60	0.04	0.1	1.0
12	Evergreen shrub	0.10	0.97	6.0	0.80	0.10	1.0	1.0
13	Deciduous shrub	0.20	0.97	6.0	0.80	0.10	1.0	1.0
14	Mixed woodland	0.15	0.96	6.0	0.80	0.80	20.0	2.0
15	Crop/mixed farming	0.20	0.95	6.0	0.85	0.06	0.7	1.0
16	Irrigated crop	0.18	0.95	6.0	0.80	0.06	0.7	1.0
17	Bog or marsh	0.12	0.98	6.0	0.80	0.03	1.0	1.0
18	Evergreen needleleaf forest	0.06	0.97	6.0	0.80	0.98	10.2	1.0
19	Evergreen broadleaf forest	0.08	0.95	6.0	0.90	2.21	20.7	1.2
20	Deciduous needleleaf forest	0.06	0.95	6.0	0.80	0.92	9.2	1.0
21	Deciduous broadleaf forest	0.09	0.95	6.0	0.80	0.91	7.2	1.2
22	Mixed cover	0.07	0.96	6.0	0.80	0.87	6.5	1.1
23	Woodland	0.08	0.96	5.7	0.80	0.83	7.4	1.0
24	Wooded grassland	0.18	0.96	5.0	0.80	0.51	3.6	1.0
25	Closed shrubland	0.10	0.97	5.1	0.63	0.14	1.4	0.7
26	Open shrubland	0.12	0.97	6.0	0.22	0.08	0.2	0.6
27	Grassland	0.11	0.96	2.6	0.73	0.04	0.2	0.7
28	Cropland	0.10	0.95	6.0	0.84	0.11	0.2	0.7
29	Bare ground	0.16	0.86	0.7	0.07	0.05	0.2	0.5
30	Urban and built-up	0.15	0.90	4.8	0.74	0.80	1.1	0.8
31	Urban1[a]	0.13	0.90	0.7	0.07	0.80	1.1	0.5
32	Urban2[a]	0.18	0.90	0.7	0.07	0.80	1.1	0.5
33	Urban3[a]	0.23	0.90	0.7	0.07	0.80	1.1	0.5
34	Urban4[a]	0.28	0.90	0.7	0.07	0.80	1.1	0.5
35	Urban5[a]	0.33	0.90	0.7	0.07	0.80	1.1	0.5
36	Urban_Green[a]	0.11	0.96	2.6	0.07	0.80	1.1	0.5

Lai, leaf area index; vfrac, vegetation fraction; zo, surface roughness; zdisp, vertical displacement; rootdep, root depth.
[a]Additional land cover/land use classes added for this study.

the link between the remote-sensing data and the atmospheric model are given in Comarazamy et al. [27], Comarazamy and González [21] and Comarazamy et al. [28].

Urban areas within the region of interest were identified using the sensor's visible spectrum, resulting in a configuration that closely resembles current land development, land use and urban sprawl mapping in Puerto Rico [36]. Optical information corresponding to these urban areas was then obtained from its thermal spectrum to create new urban and built-up land classes, classes 31–35 in Table 2, producing an improvement in the representation of the urban areas and to update model input surface characteristics [27]. Analysis of past and present LCLU information indicates a large increase in urbanized areas and a shift from a more agriculture-based economy [34, 36–38], with a ∼34% conversion rate of the surface covered by urbanization and natural vegetation (i.e. shrub land, forest and woodland), from that of agricultural lands (Figure 4).

2.2 Atmospheric model general description and configuration

An ensemble of numerical atmospheric model simulations was performed to separate the signals discussed before (i.e. LCLU change and global climate change). The model chosen was RAMS, a highly versatile numerical code developed at Colorado State University to simulate and forecast meteorological phenomena [39, 40]. The version of RAMS used in this investigation, v.4.3, contains an explicit cloud microphysics module with eight hydrometeor types and the prognostic number concentration of cloud droplets through activation of cloud condensation nuclei [41].

The simulations are centered on the northeastern region of Puerto Rico, focusing on the SJMA and the Luquillo Experimental Forest (LEF), locally referred to as El Yunque, and with three nested grids (Figure 2). Grid 1 covers the Caribbean Basin with a

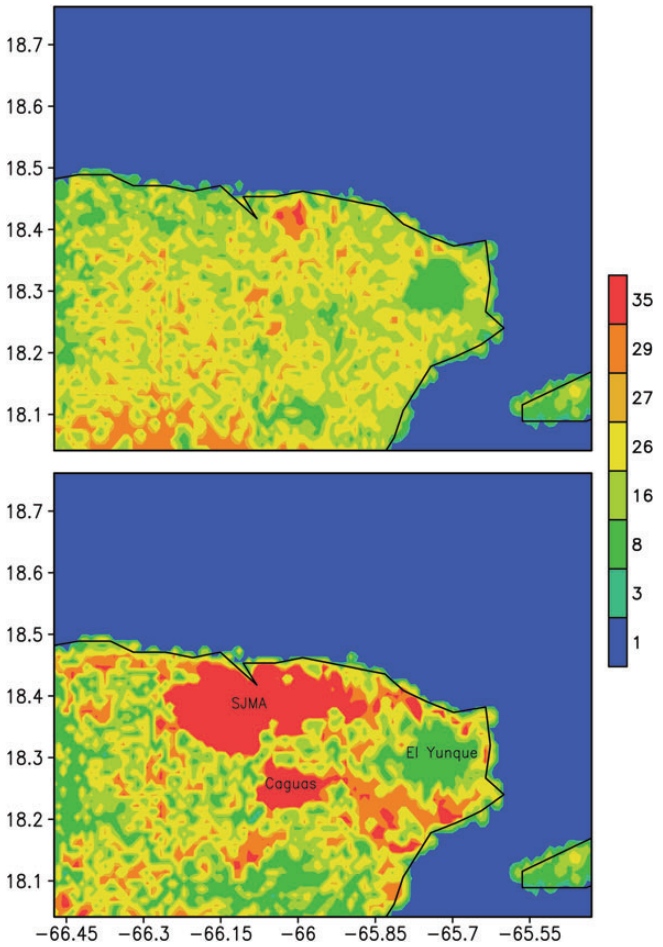

Figure 3. *PAST (top panel) and PRESENT (bottom panel, also referred as the 2000 + ATLAS scenario) surface characteristic specifications used with the two large-scale atmospheric condition scenarios described in Table 1 for Grid 3. Similar land classes were grouped together for visualization purposes (e.g. urban classes, forest classes and grassland with herbaceous agriculture). The SJMA, the Caguas residential area and El Yunque are shown in the bottom panel.*

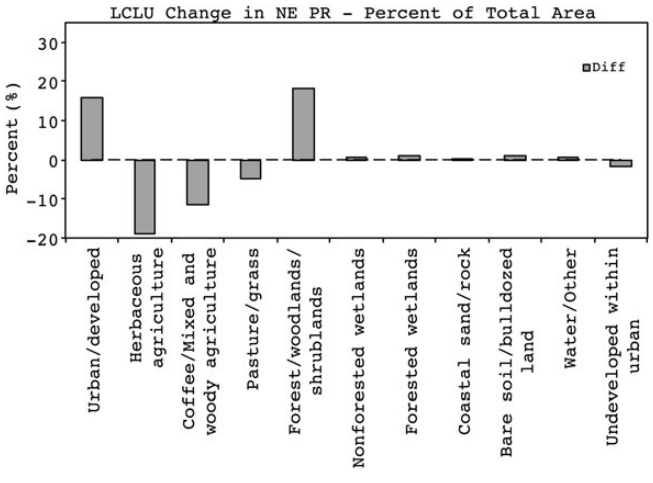

Northeastern Puerto Rico

Description	class	1951	2000	Diff
Background/water	0			
Urban/developed	30	1.92	17.81	15.89
Herbaceous agriculture	8	19.19	0.09	-19.10
Coffee/Mixed and woody agriculture	12	12.38	0.76	-11.62
Pasture/grass	27	33.73	28.99	-4.74
Forest/woodlands/shrublands	3	9.37	27.43	18.06
Nonforested wetlands	16	0.00	0.76	0.76
Forested wetlands	19	0.00	1.08	1.08
Coastal sand/rock	26	0.00	0.14	0.14
Bare soil/bulldozed land	29	0.00	0.91	0.91
Water/Other	1	0.23	0.93	0.70
Undeveloped within urban	7	1.71	0.00	-1.71

Figure 4. *Histogram of historical LCLU changes in percent of total area covered from 1951 to 2000 (top panel) and description of the most relevant vegetation and land classes with percent change and conversion rates (bottom panel) (adapted from [28]).*

horizontal resolution of 25 km and 10^4 horizontal grid points. Grid 2, which is nested within Grid 1, covers the island of Puerto Rico with 3100 horizontal grid points at a resolution of 5 km. Grid 3, with 9184 horizontal grid points and a 1 km resolution, is nested within Grid 2 and covers the SJMA, LEF, non-developed regions west and south of the city, and ocean areas to the north. The vertical grid has a grid spacing (Δz) of 30 m near the surface and then is stretched at a constant ratio of 1.15 until $\Delta z = 1000$ m. The depth of the model reaches ~26 km. A model-derived variable time step (Δt) was specified for all grids; initially, Δt was calculated as 60 s for Grid 3.

All runs are performed during the Caribbean ERS period from April to June of each year of the two timeframes selected, and for each LCLU and atmospheric condition scenario. This translates to a total of 20 three-month long simulations, where four five-year model-produced climatologies, one for each run in Table 1, were used in all validation and analysis exercises. This procedure of calculating a five-year average assures that the analysis is done with datasets where possible year-to-year variations are eliminated. The ERS is the most convenient time to study UHI effects in northeastern Puerto Rico [15], during which the atmospheric model has previously performed satisfactorily [28, 42]. A spin-up time of one week at the start of each three-month simulation is specified to allow numerical stabilization of the main atmospheric model, sub-models and parameterizations.

After all input information and parameters were incorporated into the atmospheric model and the simulations were performed, the five-year average of daily minimum and maximum temperatures from the PRESENT1 and PAST2 simulations (see Table 1) was validated satisfactorily when compared with corresponding observed values from surface COOP stations located within the SJMA and LEF, following procedures developed for the same model applied to the region of interest [21, 27, 28, 42].

3 THERMAL RESPONSE NUMBER

As the current release of atmospheric mesoscale model used, and the general surface energy budget model that is part of it, does not completely account for the thermal effects of heat storage or soil heat flux, and the LCLU characterization in RAMS uses a

structural classification based on land cover classes and not on a functional classification to assess the impact of land cover in model results, a classifier is needed for the determination of the surface energy budget derived from surface or near-surface temperatures for the various types of surfaces in a particular area. One feasible approach would be the use of the TRN developed by Luvall and Holbo [43] and applied to different surface types. The TRN is a surface property defined as the ratio of the surface net radiation, which integrates the effects of the non-radiative fluxes over short periods of time and the rate of change in surface temperature, which expresses how those fluxes are reacting to radiant energy inputs.

The TRN (J m^{-2} $°C^{-1}$) is then defined as follows:

$$\mathrm{TRN} = \frac{(R_n \Delta t)}{\Delta T}, \tag{1}$$

where $(R_n \Delta t)$ represents the net radiation, R_n, over a time interval Δt, and ΔT is the change in mean temperature for each surface type during Δt. A Δt of 1 h is used in this research.

Then, in Equation (1) R_n expresses the combined energies of the non-radiative surface processes and how these are partitioned at the surface following:

$$R_n = (1 - a)R_s \downarrow + R_l \downarrow + R_l \uparrow = H + \mathrm{LE} + G, \tag{2}$$

where a is the surface's albedo; $R_s\downarrow$, $R_l\downarrow$ and $R_l\uparrow$ are the incident surface flux of shortwave and longwave radiation and the upward surface flux of longwave radiation, respectively; H is the surface sensible heat flux; LE the surface latent heat flux and G, the surface storage term or soil heat flux. This is a similar approach as the estimates of G derived as residuals in Equation (2) and an objective hysteresis model applied to urban surfaces in previous studies [3, 44, 45].

The thermal response of an urban landscape may involve such surfaces as uniform asphalt parking lots, areas of high-rise steel and glass buildings or residential areas with trees and lawns. The partitioning of energy budget terms depends on these surface types. In natural landscapes, the partitioning depends on canopy biomass, leaf area index and moisture status, all of which vary according to the development stage of the ecosystem. In all cases investigated here, LCLU changes substantially altering the surface energy budget. Large TRN values mean that more energy is required to increase that surface's temperature [46]. Areas that have mostly vegetated surfaces have a greater TRN than completely barren or built-up surfaces because the net radiation processed by the surface is mostly used for latent heat (evaporation of water) rather than sensible heat (heating the air), effectively producing a small ΔT over Δt for these types of surfaces. TRN values are useful in determining evapotranspiration and surface heat flux characteristics for common urban surfaces, and for assessing the thermal dynamics of these surfaces throughout the day [43, 47].

4 IMPACT OF URBANIZATION AND GLOBAL WARMING ON SURFACE ENERGY PARTITIONING IN A TROPICAL CITY

To study the impacts of LCLU changes and GW on surface energy balance terms in a tropical city, the northeastern region of the Caribbean island of Puerto Rico was taken as the test case. As with the validation, the results presented in the next subsections refer to the five-year climatology of each of the simulation scenarios described in Table 1. To better guide the reader through these scenarios, they are described as follows:

PRESENT1: present LCLU + actual GW conditions
PRESENT2: present LCLU + pre-GW conditions
PAST1: past LCLU + actual GW conditions
PAST2: past LCLU + pre-GW conditions

4.1 Long-term climate impacts

The 1 km × 1 km resolution of the model grid used for this research does not allow for the identification of individual surface elements (e.g. buildings, parking lots, streets and trees); thus to analyze the thermal response of different surfaces, as well as the impact of LCLU changes and global climate change on the TRN, the SJMA and El Yunque are taken as regions representing heavily urbanized and vegetated/forested surfaces, respectively (see Figure 3).

Results for the TRN in the region occupied by the SJMA show how the presence of the city in the PRESENT1 and PRESENT2 simulations produces lower values than the simulations with a pre-urban land specification, PAST1 and PAST2, throughout the Caribbean ERS, showing ∼100–200 kJ m^{-2} $°C^{-1}$ against ∼200–400 kJ m^{-2} $°C^{-1}$, respectively, both with a positive slope as the season progresses (Figure 5, top left). This difference might be due to an increase in sensible heat flux in the urban scenarios related to an increase in surface temperature, which in turn raises air temperatures, as seen in the air temperature differences shown in Comarazamy et al. [28]. The increasing pattern is a response to increasing moisture available in the atmosphere in the onset of the summer season. The partitioning of energy is analyzed using the model results for sensible and latent heat flux to calculate the Bowen ratio, B, defined as the ratio of the sensible to latent heating, H/LE. The total change in B, PRESENT1 vs. PAST2, shows that there is more latent heat flux via evapotranspiration in the pre-urban scenarios and more sensible heat flux producing larger surface ΔT values over Δt in the urban scenarios (Figure 5, top right).

By analyzing the TRN and B patterns of the simulation with constant LCLU, it is concluded that changes in the thermal response of such surface are associated with increases in sensible heat flux in the simulations driven with present atmospheric conditions. Interesting results arise when comparing the simulations that produce similar B patterns, where it can be seen that major changes in the relationship between sensible and latent

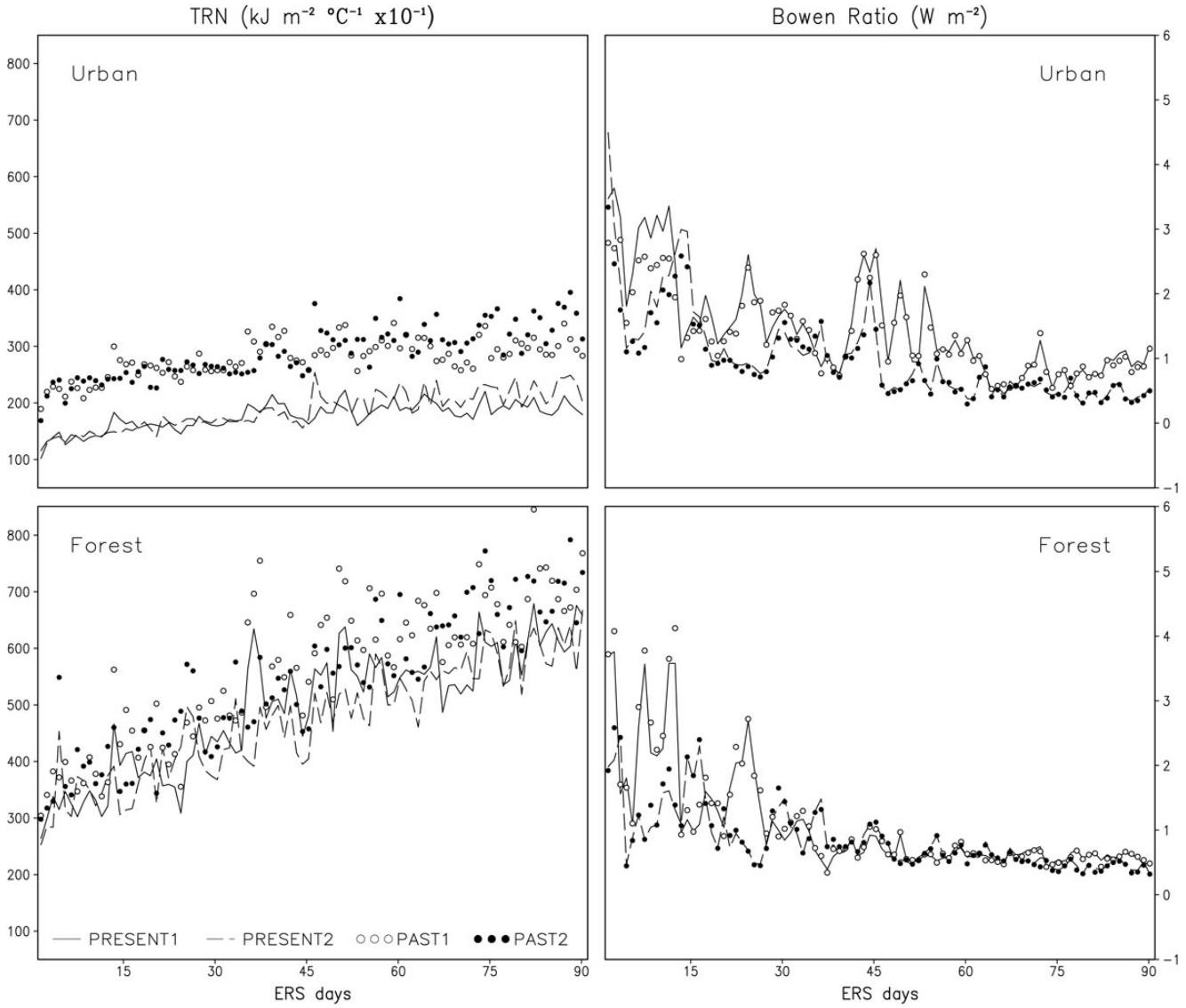

Figure 5. *Time series of daily TRN (kJ m^{-2} $°C^{-1}$) (left panels) and Bowen ratio values (right panels) during the Caribbean ERS, calculated for the SJMA (top) and El Yunque (bottom). In all panels, the four simulations in Table 1 are shown, describing the runs with present LCLU and present atmospheric conditions (solid line), with present LCLU and past atmospheric conditions (dashed line), with past LCLU and present atmospheric conditions (open circles) and with past LCLU and past atmospheric conditions (closed circles).*

heat fluxes are due to changes in atmospheric conditions, proving that there are drier atmospheric conditions during the present timeframe than in the past, results that are in agreement with reported changes in the hydrological cycle of northeastern Puerto Rico [21]. Taking for example the PRESENT1 and PAST1 simulations having the same B pattern, and given that PRESENT1 has a much lower thermal response, then to maintain energy balance, the simulation with an urban representation must have increased thermal storage (G) in the SJMA region. Similar conclusions can be drawn from the results for the urbanized residential area of Caguas (not shown but included in the calculation for urban presented in Figure 5), with the distinction that the TRN and B have more variability here, which might be due to the presence of more sub-grid vegetation patches in the urban cells in the Caguas region.

The montane cloud forest of El Yunque shows higher *TRN* values than the urban areas, and a much more pronounced increasing slope throughout the ERS, from $\sim$300 kJ m^{-2} $°C^{-1}$ to between 700 and 800 kJ m^{-2} $°C^{-1}$ (Figure 5, bottom left). These results show how the forest still manages to consistently use more energy for evapotranspiration, increasing the latent heat flux in all scenarios ($B < 1$) for a great portion of the ERS (Figure 5, bottom right), in spite of having higher cloud base heights and decreased accumulated precipitation [21]. Also, the TRNs produced by the past LCLU specifications are higher than those for the runs with present surface characteristics in El

Yunque, although not as marked a difference as for the urban areas, where LCLU changes are far more dramatic.

In general, it is shown how the TRN provides a good measure of how a surface reacts to different radiative inputs in terms of surface temperature change over short periods of time, and how this is related to the way each surface type is partitioning the net surface radiation into non-radiative energies by applying the residuals approach to the surface energy balance terms (H, LE, G). It also provides an excellent indicator of local and regional environmental change that could be used to test different mitigation and adaptation strategies, depending on how the thermal response of a particular area changes to the application of such strategies.

4.2 Effectiveness of mitigation strategies

In order to test the effectiveness of different mitigation strategies for the quantified effects of long-term urbanization in the SJMA, a series of short weather simulation were configured and executed. The mitigation strategies tested were the use of green roofs throughout the city and the inclusion of widespread urban vegetation within the urban core. For all weather modification cases spanning 48 h, the same driving atmospheric conditions were used for the corresponding scenarios. The LCLU specifications for the base case (ATLAS) were specified as shown in the bottom panel of Figure 3, representing the actual urban extension and characteristics of the SJMA, against which all mitigation strategies are compared with. These simulations ran for 48 h, 06 to 08 November 2012, driving the model with historical radiosonde data from regular launches at the San Juan International Airport and updated every 12 h. Early November is another convenient time of the year for studying the local effects of urbanization and proposed mitigation strategies because it is towards the end of the hurricane season and the onset of the dry season.

For the green roof test, the SJMA and Caguas regions maintained the same horizontal configuration as the base case, but with the biophysical parameters of Urban_Green (class 36 in Table 2) throughout all urban areas. Here the 'green roofs' are specified by patches of grass located at the top of buildings within the urban areas, represented by combining the biophysical parameters of grass and concrete, while keeping the mechanical mixing parameters (surface roughness and vertical displacement) of the urban landscape. Results from these simulations show that the 'green roof' configuration serves to greatly alleviate the elevated air temperatures produced by an urban area with a high concrete density by 1–1.5°C (Figure 6, bottom panel). In terms of the partitioning of surface energy balance terms, it is also shown how the green roofs help in increasing the latent heat flux and reduces sensible heat flux exchange with the atmosphere, evident in the low B values that it produced during the simulation period (Figure 7). When B is less than one, a greater proportion of the surface available energy is exchanged to the atmosphere as latent heat flux than as sensible heat flux, inversely when sensible heat flux transfer is larger than latent heat flux, B obtains values

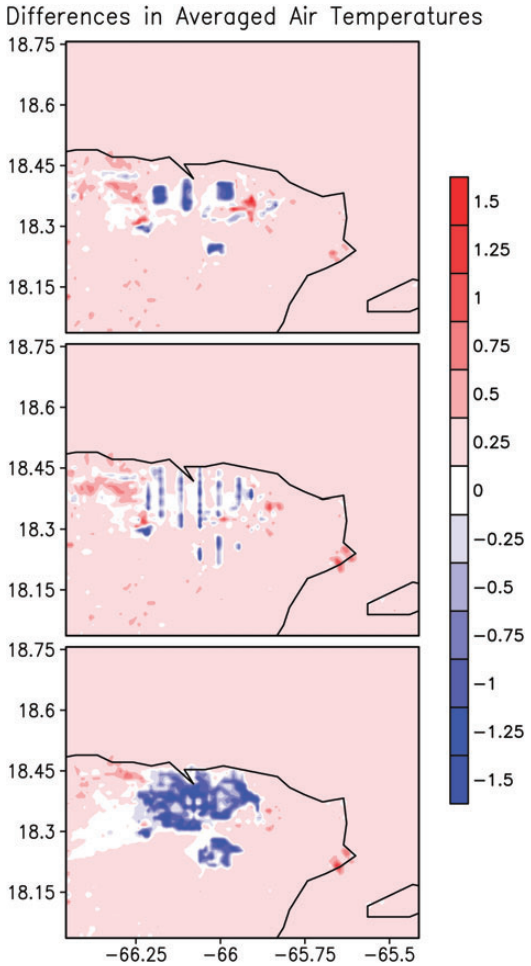

Figure 6. *Spatial distribution of averaged air temperature differences (°C) at 2 m AGL between the Parks (top), Trees (center) and green roofs (bottom) scenarios simulated for the analysis as compared with the simulations driven with the 2000 + ATLAS land use classification in Figure 3.*

greater than 1. As LE approaches zero, B becomes unbounded, a result typical of heavily urbanized areas and some barren surfaces. In the SJMA, an urban area with an extremely high concrete density, the inclusion of green roofs produced B less than 1. This mitigating impact could be greatly enhanced when the effects of plant processes and water budget changes are taken into account.

The configuration that incorporates vegetation within the urban core helps in quantifying the effects of natural processes while testing the mitigation capacity of two scenarios: the presence of tree-lined avenues and the construction of large parks in the SJMA and Caguas, hereafter referred to as Trees and Parks, respectively. The two scenarios in this configuration are constructed by a complete replacement of the urban cells by trees (Evergreen broadleaf, class 19 in Table 2), a logical scenario for the Parks case, not so much for the Trees case, but in order to have the same percentage of vegetation incorporated in each case (~18%) and do a fair comparison of modeling results and effects, entire bands of 1×1 km^2 cells were introduced as vegetation for the later case.

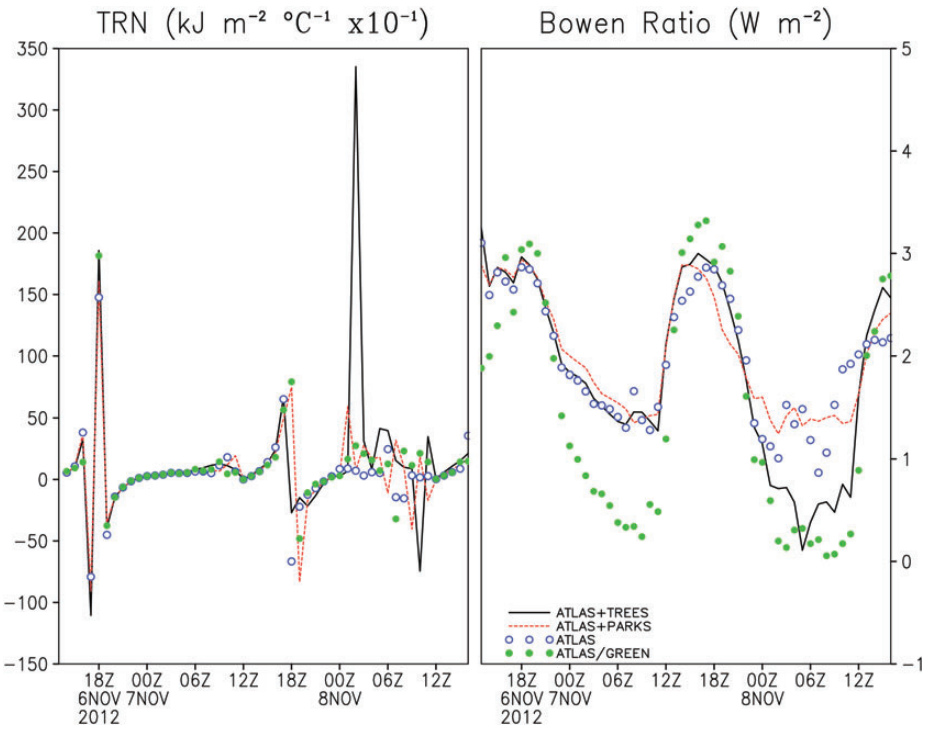

Figure 7. *Time series of hourly TRN (kJ m^{-2} $^{\circ}C^{-1}$) (left panel) and Bowen ratio values (right panel) calculated for the SJMA and Caguas during the 48-h simulation period starting on February 10, 2012. In both panels, the three simulations for February 2012 (Table 1) are shown, describing the green roofs (solid green dots), Trees (solid black line), Parks (dashed red line) and base Atlas (open blue circles) scenarios.*

Results for averaged air temperatures show that the two urban vegetation scenarios greatly reduce temperatures (∼1–1.2°C) over the urbanized areas and immediate surroundings within the SJMA and Caguas when compared with the simulation executed with the base 2000 + ATLAS LCLU classification (Figure 6, top and center panels). All simulations are driven by the same atmospheric conditions. One conclusion that is drawn from these results, in light of the practical application of the proposed mitigation strategies, is that the Trees scenario is more feasible than the construction of extremely large parks in an urban area with an already high building and concrete density. It is also shown that the Trees case is more efficient in its use of energy and partitioning of surface energy budget terms, as shown in the TRN and Bowen ratio results, especially towards the end of the simulation period when a spike in TRN, possibly due to less energy being stored and surface temperature decreasing rapidly, and a dip in *B*, less sensible heat flux over latent heat (Figure 7). In general, these results show that green roofs and urban vegetation have a profound effect on the area's air temperature and surface energy balance, producing lower temperatures and storing less energy, partitioning energy as latent heat more efficiently. These results deem the inclusion of green roofs throughout the urban area as the most efficient mitigating strategy for the observed UHI effects, followed by the lining of streets with appropriate vegetation for the region where the city is situated and the construction of large parks. It is worth noting again that some secondary effects of these mitigation strategies were not included in the study, like the water balance impact of green roofs and the social impacts of inner city recreational parks.

5 SUMMARY AND CONCLUSION

The work presented here is an investigation of the climate impacts of LCLU changes and GW on the surface energy balance of a coastal tropical city, using the RAMS as the main research tool and taking the SJMA, Puerto Rico, as the test case. The impact analysis is performed for long-term effects as well as short-term effects.

The numerical modeling simulation matrix for the long-term study combines two large-scale atmospheric conditions to drive the model and two LCLU scenarios for the corresponding atmospheric timeframes that provide the surface characteristics. The two five-year periods from 1955 to 1959, for the past conditions, and from 2000 to 2004, for the present conditions, were selected under a series of criteria that minimizes the influences of global scale oscillations (e.g. ENSO and NAO) on Caribbean ERS climate, which represents a significant climate change in the region of interest and that are in accordance with historical LCLU changes in Puerto Rico. The NCEP Reanalysis 2.5° 6-hourly data and the Smith and Reynolds ERSST v3b monthly data provided the large-scale atmospheric and oceanic conditions, respectively. The LCLU specifications for each period were obtained from digital maps of vegetation cover for 1951 and

2000, with the present specifications complemented by remote-sensing information gathered in early 2004 to have a better representation of the current urban areas located in the modeling domain.

In terms of the long-term impacts due to LCLU changes in tropical coastal regions, model results show that the TRN of the area occupied by the SJMA has decreased as a consequence of replacing the lowland coastal plain vegetation with man-made materials, indicating that it takes less energy to raise the surface temperature of the region in question, whereas the thermal response of the forested region has remained virtually unchanged. The GW signal also has effects on the thermal response of the region occupied by the SJMA, where the dryer present conditions generate lower TRN values than in the past climate conditions for both LCLU cases. These differences from the GW signal are more evident in the Bowen ratio pattern for the simulation driven by the present atmospheric and SST conditions and in those driven with past climate conditions. Differences in the thermal response of the forest due to global climate changes are less evident, with the exception of the onset of the ERS, when the pattern in the Bowen ratio follows the same pattern as in the urban area. There were also reported changes in air temperature and precipitation obtained with the same climate reconstruction and factor separation technique [21, 28].

There is a myriad of secondary and tertiary social, economic and cultural implications of the total climate change due to the combine effects of LCLU changes and GW in coastal tropical regions. This is the main reason why comprehensive research like the one described in this document is of extreme importance. The inclusion of adaptation and mitigation strategies that may have a significant impact is a necessary step in completing the LCLU analysis. Some of these mitigation strategies were tested in the work presented here. Green roofs and vegetation canopy incorporated into a heavily urbanized city are proven to have a significant mitigating potential and impact, not only reducing observed air temperatures, but also improving the efficiency with which the urban area uses and partitions surface energy balance terms.

To improve the results presented in this document, an investigation of parameters that can be extracted from remote-sensing information to update the atmospheric model surface characteristics should be performed. Parameters such as albedo, emissivity, surface roughness, leaf area index and vegetation fraction, among other surface characteristics, as well as other important parameters used in regional atmospheric modeling, like skin/canopy temperature, volumetric soil moisture content and soil textural class, could be incorporated into the measurements obtained by the next generation of remote sensors, like the Hyperspectral-Infrared Imager (HyperIRI).

Projections for future climate changes in tropical coastal regions could be performed using different GHG emissions scenarios [48] combined with statistical and dynamical modeling of LCLU change and urban growth [15, 49, 50]. Downscaled and detailed climate change projections are a priority to be able to establish critical mitigation and adaptation policies. The findings discussed in this document apply to late 20th century urbanization and climate change, a period what saw a dramatic expansion of urbanization and other cases of LCLU changes in Puerto Rico, and only modest large-scale warming. The implications would be that if the warming continues, presuming that urbanization has reached a relative stable extent (and may see some reduction of its impact as shown in the modeling results due to expansion of reflective and green roofs, greater urban vegetation, reforestation programs, etc.), the future will not show the same relative effects as experienced during the long-term period presented in this document.

ACKNOWLEDGEMENTS

NOAA funded this research under CREST grant NA06OAR4810162. The atmospheric model simulations were performed at the High Performance Computing Facilities of the University of Puerto Rico at Río Piedras.

REFERENCES

[1] Landsberg HE. *The Urban Climate*. Academic Press, 1981, 275 pp.
[2] Oke TR. *Boundary Layer Climates*. Routledge, 1987, 464 pp.
[3] Grimmond CSB, Oke TR. Heat storage in urban areas: local-scale observations and evaluation of a simple model. *J Appl Meteorol* 1999;**38**:922–40.
[4] Masson V. A physically-based scheme for the urban energy budget in atmospheric models. *Bound-Lay Meteorol* 2000;**94**:357–97.
[5] Martilli A, Clappier A, Rotach MW. An urban surface exchange parameterisation for mesoscale models. *Bound-Lay Meteorol* 2002;**104**:261–304.
[6] Jauregui E, Romales E. Urban effects on convective precipitation in Mexico City. *Atmos Environ* 1996;**30**:3383–9.
[7] Jauregui E. Heat island development in Mexico City. *Atmos Environ* 1997;**31**:3821–31.
[8] Noto K. Dependence of heat island phenomena on stable stratification and heat quantity in calm environment. *Atmos Environ* 1996;**30**:475–85.
[9] Dixon PG, Mote TL. Patterns and causes of Atlanta's urban heat island-initiated precipitation. *J Appl Meteorol* 2003;**42**:1273–84.
[10] Ochi S, Uchihama D, Takeuchi W, *et al*. Monitoring urban heat environment in East Asia. *GIS Development* 2002;**6**:18–20.
[11] Rozoff CM, Cotton WR, Odegoke JO. Simulation of St. Louis, Missouri, land use impacts on thunderstorms. *J Appl Meteorol* 2003;**42**:716–38.
[12] Inoue T, Kimura F. Urban effects on low-level clouds around the Tokyo metropolitan area on clear summer days. *Geophys Res Lett* 2004;**31**:L05103.
[13] Shepherd JM. A review of current investigations of urban-induced rainfall and recommendations for the future. *Earth Interact* 2005;**9**:1–27.
[14] Tso CP. A survey of urban heat island studies in two tropical cities. *Atmos Environ* 1996;**30**:507–19.
[15] Velazquez-Lozada A, Gonzalez JE, Winter A. Urban heat island effect analysis in San Juan, Puerto Rico. *Atmos Environ* 2006;**40**:1731–41.
[16] Lawton RO, Nair US, Pielke RA, Sr, *et al*. Climatic impact of tropical lowland deforestation on nearby montane cloud forests. *Science* 2001;**294**:584–7.
[17] Nair US, Lawton RO, Welch RM, *et al*. Impact of land use on Costa Rican tropical montane cloud forests: sensitivity of cumulus cloud field characteristics to lowland deforestation. *J Geophys Res* 2003;**108**(D7):4206.

[18] Ray DK, Nair US, Lawton RO, *et al*. Impact of land use on Costa Rican tropical montane cloud forests: Sensitivity of orographic cloud formation to deforestation in the plains. *J Geophys Res* 2006;**111**:D02108.

[19] Van der Molen MK. Meteorological impacts of land use change in the maritime tropic. PhD Thesis, Vrije Universititeit Amsterdam. 2002; 262 pp. (available at http://www.geo.vu.nl/~moli/).

[20] Van der Molen MK, Dolman AJ, Waterloo MJ, *et al*. Climate is affected more by maritime then by continental land use change: a multiple scale analysis. *Global Planet Change* 2006;**54**:128–49.

[21] Comarazamy DE, González JE. Regional long-term climate change (1950–2000) in the Midtropical Atlantic and its impacts on the hydrological cycle of Puerto Rico. *J Geophys Res* 2011;**116**:D00Q05.

[22] Daly C, Helmer EH, Quiñones M. Mapping the climate of Puerto Rico, Vieques and Culebra. *Int J Climatol* 2003;**23**:1359–81.

[23] Taylor MA, Enfield DB, Chen AA. Influence of the tropical Atlantic versus the tropical Pacific on Caribbean rainfall. *J Geophys Res* 2002;**107**:10.1–10.14.

[24] González JE, Luvall JC, Rickman D, *et al*. Urban heat islands developing in coastal tropical cities. *EOS Transact AGU* 2005;86, 42, pp. 397 & 403.

[25] González JE, Luvall JC, Rickman D, *et al*. Urban heat island identification and climatological analysis in a coastal, tropical city: San Juan, Puerto Rico. In Weng Q, Quattrochi D (eds). *Urban Remote Sensing*. CRC Press, 2006, 223–52.

[26] Imamura IR. Role of soil moisture in the determination of urban heat island intensity in different climate regimes. *Trans Ecol Environ* 1993;**1**: 395–402.

[27] Comarazamy DE, González JE, Luvall JC, *et al*. A land-atmospheric interaction study in the coastal tropical city of San Juan, Puerto Rico. *Earth Interact* 2010;**14**:1–24.

[28] Comarazamy DE, González JE, Luvall JC, *et al*. Climate impacts of land-cover and land-use changes in tropical islands under conditions of global climate change. *J Climate* 2013;**26**:1535–50.

[29] Chen AA, Taylor MA. Investigating the link between early season Caribbean rainfall and the El Niño+1 year. *Int J Climatol* 2002;**22**:87–106.

[30] Malmgrem BA, Winter A, Chen D. El Niño-southern oscillation and North Atlantic oscillation control of climate in Puerto Rico. *J Climate* 1998;**11**:2713–7.

[31] Kalnay E, Kanamitsu M, Kistler R, *et al*. The NCEP/NCAR 40-year reanalysis project. *B Am Meteorol Soc* 1996;**77**:437–71.

[32] Smith TM, Reynolds RW. Extended reconstruction of global sea surface temperatures based on COADS data (1854–1997). *J Climate* 2003; **16**:1495–510.

[33] Smith TM, Reynolds RW, Peterson TC, *et al*. Improvements to NOAA's historical merged land-ocean surface temperature analysis (1880–2006). *J Climate* 2008;**21**:2283–96.

[34] Kennaway T, Helmer EH. The forest types and ages cleared for land development in Puerto Rico. *GISci Remote Sens* 2007;**44**:356–82.

[35] Dickinson RE, Sellers AH, Kennedy PJ, *et al*. Biosphere-Atmosphere Transfer Scheme (BATS) for the NCAR Climate Community Model. Technical Note NCAR/TN-275+STR. 1986, 69 pp.

[36] Martinuzzi S, Gould WA, Ramos González OM. Land development, land use, and urban sprawl in Puerto Rico integrating remote sensing and population census data. *Landscape Urban Plan* 2007;**79**:288–97.

[37] Helmer EH. Forest conservation and land development in Puerto Rico. *Landscape Ecol* 2004;**19**:29–40.

[38] Lugo AE, Helmer E. Emerging forests on abandoned land: Puerto Rico's new forests. *Forest Ecol Manag* 2004;**190**:145–61.

[39] Pielke RA, and coauthors. A comprehensive meteorological modeling system—RAMS. *Meteorol Atmos Phys* 1992;**49**:69–91.

[40] Cotton WR, Pielke RA, Sr, Walko RL, *et al*. RAMS 2001: current status and future directions. *Meteorol Atmos Phys* 2003;**82**:5–29.

[41] Saleeby MS, Cotton WR. A large-droplet mode and prognostic number concentration of cloud droplets in the Colorado State University Regional Atmospheric Modeling System (RAMS) Part I: module descriptions and supercell test simulations. *J Appl Meteorol* 2004;**43**:182–95.

[42] Comarazamy DE, González JE. On the validation of the simulation of early season precipitation on the island of Puerto Rico using a mesoscale atmospheric model. *J Hydrometeorol* 2008;**9**:507–20.

[43] Luvall JC, Holbo HR. Measurement of short-term thermal responses of coniferous forest canopies using thermal scanner data. *Remote Sens Environ* 1989;**27**:1–10.

[44] Grimmond CSB, Cleugh HA, Oke TR. An objective heat storage model and its comparison with other schemes. *Atmos Environ* 1991;**25B**:311–26.

[45] Roberts SM, Oke TR, Grimmond CSB, *et al*. Comparison of four methods to estimate urban heat storage. *J Appl Meteorol Clim* 2006;**45**:1766–81.

[46] Luvall JC, Lieberman D, Lieberman M, *et al*. Estimation of tropical forest canopy temperatures, thermal response numbers and evapotranspiration using an aircraft-based thermal sensor. *Photogramm Eng Rem S* 1990;**56**:1393–401.

[47] Luvall JC. The use of remotely sensed surface temperatures from an aircraft-based thermal infrared multispectral scanner (TIMS) to estimate the spatial and temporal variability of latent heat fluxes and thermal response numbers from a white pine (Pinus strobus L.) plantation. In Quattrochi DA, Goodchild MF (eds). *Scale in Remote Sensing and GIS*. CRC Press, 1997, 169–85.

[48] Meehl GA, Stocker TF, Collins WD, *et al*. Global climate projections. In Solomon S, Qin D, Manning M, Chen Z, Marquis M, Averyt KB, Tignor M, Miller HL (eds). *Climate Change 2007: The Physical Science Basis. Contribution of Working Group I to the Fourth Assessment Report of the Intergovernmental Panel on Climate Change*. Cambridge University Press, 2007.

[49] López E, Bocco G, Mendoza M, *et al*. Predicting land-cover and land-use change in the urban fringe: a case in Morelia city, Mexico. *Landscape Urban Plan* 2001;**55**:271–85.

[50] de Almeida CM, and coauthors. GIS and remote sensing as tools for the simulation of urban land-use change. *Int J Remote Sens* 2005;**26**:759–74.